Heliyon 10 (2024) e36725

Contents lists available at ScienceDirect

Heliyon

journal homepage: www.cell.com/heliyon

Research article

Evaluation of zirconia ceramics fabricated through DLP 3d printing process for dental applications

Muneer Khan Mohammed [a,**], Abdulrahman Alahmari [b,*], Hisham Alkhalefah [a], Mustufa Haider Abidi [a]

[a] Advanced Manufacturing Institute, King Saud University, PO Box 800, Riyadh, 11421, Saudi Arabia
[b] Industrial Engineering Department, King Saud University, PO Box 800, Riyadh, 11421, Saudi Arabia

ARTICLE INFO

Keywords:
Zirconia
Ceramics
3d printing
Mechanical properties
Characterization
Additive manufacturing

ABSTRACT

Zirconia ceramics are versatile materials with remarkable properties such as a high thermal resistance, high fracture strength, and low thermal conductivity. They are chemically inert and highly wear- and corrosion-resistant, making them ideal for a wide range of applications in the aerospace, automotive, and biomedical fields. In dentistry, zirconia ceramics are used for veneers, crowns, bridges, and implants because of their biocompatibility. Despite the various benefits of zirconia ceramics, they are difficult to process because of their high hardness and brittleness. Additive manufacturing (AM) has proven to be a viable alternative to conventional fabrication processes, particularly for the processing of difficult-to-cut materials. AM of ceramics has gained significant attention in recent years because of its flexibility and ability to produce customized geometries rapidly and economically. In this study, the digital light processing (DLP) technique was employed to 3D print yttria-stabilized zirconia. The fabricated zirconia was evaluated and characterized for use in dental applications. Thermogravimetric analysis (TGA) and differential thermogravimetry (DTG) were performed on the green body to assess the decomposition of the additives in the slurry and determine the debinding temperatures. The as-built parts were subjected to debinding and sintering to obtain fully dense zirconia parts. The parts tended to shrink after sintering; therefore, the shrinkage ratios were evaluated and found to be 1.2817, 1.2900, and 1.3388 in the x-, y-, and z-directions, respectively. The average density after sintering was 6.031 g/cc. The flexural strength determined using four-point bending tests was 451.876 MPa, and the tensile and compressive strengths were 143 MPa and 298.4 MPa, respectively.

1. Introduction

Zirconium dioxide (ZrO_2), also known as zirconia, is derived from the naturally occurring mineral baddeleyite. Zirconia can exist in multiple crystalline structures. Pure zirconia is present in the monoclinic phase at room temperature and transforms into tetragonal and cubic phases at elevated temperatures. Pure zirconia has limited applications because it undergoes disruptive phase transformations at high temperatures. These phase transformations are associated with significant variations in volume, making zirconia brittle and prone to breakage. Zirconia is generally doped with oxides such as magnesium oxide (MgO), yttrium oxide (Y_2O_3, yttria),

* Corresponding author.
** Corresponding author.
E-mail addresses: muneerkm@ksu.edu.sa (M.K. Mohammed), alahmari@ksu.edu.sa (A. Alahmari).

https://doi.org/10.1016/j.heliyon.2024.e36725
Received 6 June 2024; Received in revised form 20 August 2024; Accepted 21 August 2024
Available online 22 August 2024
2405-8440/© 2024 The Authors. Published by Elsevier Ltd. This is an open access article under the CC BY-NC-ND license (http://creativecommons.org/licenses/by-nc-nd/4.0/).

and calcium oxide (CaO) to obtain a stable crystal structure [1]. Zirconia ceramics exhibit unique combinations of properties that make them valuable for a wide range of applications. They exhibit high strength, exceptional toughness, and wear resistance, making them ideal grinding media for ball milling. They also have a high melting point and thermal resistance; therefore, they are used in furnace linings and crucibles. Yttria-stabilized zirconia exhibits high thermal resistance, high fracture strength, and low thermal conductivity. This material is hard, chemically inert, and biocompatible. It exhibits superior corrosion and wear resistance and has a natural appearance, which makes it favorable for the fabrication of dental restorations [2,3]. Yttria-stabilized tetragonal zirconia (Y-TZP) is the most robust dental ceramic with excellent mechanical properties [4]. Based on the yttria content and manufacturing process, Y-TZP ceramics have different grades with varying strengths and translucencies [5,6]. Of these, 3 mol% Y-TZP (3Y-TZP) is the strongest and most opaque; 4 mol% yttria–partially stabilized zirconia (4Y-PSZ) is more translucent but weaker than 3Y-TZP. The grades of 5 and 6 mol% (5Y/6Y-PSZ) are the most translucent and weakest. Among these, 3Y-TZP is most commonly used in dental ceramics [7]. These materials also exhibit osteoconductive properties and are effective alternatives to traditional titanium implants in patients with metal allergies. However, some patients with titanium implants develop allergic reactions, resulting in inflammation and implant loss [8]. Therefore, dental research is currently focused on metal-free dental restorations. Moreover, In vivo and in vitro studies have suggested that zirconia is a superior alternative to titanium [9–11]. Despite the various advantages of zirconia, there are several challenges related to its processing and performance arising from its brittle nature.

In general, dental restorations are fabricated through conventional machining of pre-sintered zirconia blocks [12–14]. In this process, a die or wax pattern is first scanned to create a design model of the restoration using computer-aided design (CAD) software. The pre-sintered zirconia blocks are then milled using computer-aided manufacturing (CAM) to fabricate the restorations. Finally, the restorations are sintered at high temperature in a furnace to achieve full crystallization and attain their maximum strength [15]. However, this process is associated with milling-induced damage and surface defects. Another route for fabricating dental restorations is through the hard machining of fully dense Y-TZP blocks. The high hardness and low machinability of fully sintered zirconia make it difficult to cut; therefore, expensive tools and machining systems are required [7]. The machining of zirconia blocks, either pre-sintered or fully sintered, has drawbacks such as high material wastage, limited scope for the fabrication of intricate parts and customized geometries, and higher costs.

Additive manufacturing (AM) has proven to be a viable alternative to conventional processes, particularly for processing difficult-to-cut materials. AM is the layer-by-layer addition of material to form a near-net-shaped three-dimensional (3D) object using 3D CAD data. AM has numerous advantages over other processes, such as reduced lead times, flexibility, customization, and better material management [16]. AM has been applied in the aerospace, automotive, construction, and biomedical industries. AM of ceramics has gained significant attention in recent years because of its flexibility and ability to produce customized geometries and porous structures rapidly and economically.

Several AM techniques have been applied for the fabrication of ceramics. Two approaches can be used for AM of ceramics. One is the powder-based approach, in which ceramic powder is used as the feedstock material. The ceramic powder is bonded either with liquid binders or melted directly using a high-energy source such as a laser. Selective laser sintering (SLS)/SLM is an effective powder-based technique in which a ceramic powder is melted using a high-energy laser beam. The main advantage of the powder-based approach is that ceramics can be directly fabricated without the need for a suspension material [17]. However, the fabrication of ceramics through SLS results in low dimensional accuracy, internal porosity, and a low relative density [18]. Inkjet printing utilizes a binding liquid to bond ceramic powders to produce 3D parts [19,20]. The second method for the AM of ceramics is the slurry-based approach, in which the ceramic powder is suspended in a liquid or semi-liquid system in the form of either inks or pastes, depending on the solid loading and viscosity of the system [21]. AM techniques such as stereo lithography (SLA) [22], DLP [23], inkjet printing [24], and extrusion-based 3D printing utilize this slurry-based approach. The DLP-based AM of ceramics has shown promising results in terms of speed, dimensional accuracy, and precision [2]. AM of ceramics is challenging because of their high melting point, susceptibility to thermal shocks, and low sintering ability. In slurry-based or VAT photopolymerization-based processes, the two main challenges are optimizing the slurry composition with good rheological characteristics and optimizing the debinding and sintering schedules. To produce dense parts, the slurry should be photo-curable and homogenous with a high solid loading. In addition, to facilitate recoating during printing, the slurry should also exhibit low viscosity, good flowability, and shear-thinning behavior [25].

Most previous research related to the 3D printing of zirconia has focused on yttria-stabilized t-ZrO_2, particularly for dental applications. There are numerous applications of 3D printing in dentistry, such as for crowns, bridges, dentures, surgical guides, implants, and orthodontics materials [26]. Zirconia is biocompatible with the tissues in the oral cavity and has been reported to be osteoconductive. Thus, it facilitates bone formation when in contact with tissues. Zirconia also facilitates a significant reduction in bacterial adhesion compared with titanium implants, which has a positive effect on peri-implant soft tissues [27]. Osman et al. [2] fabricated a zirconia dental implant using a DLP-based 3D printer and evaluated its dimensional accuracy and mechanical properties. Scanning electron microscopy (SEM) analysis revealed the presence of cracks and internal porosity. Chen et al. [28] fabricated zirconium dioxide (ZrO_2) teeth using a DLP-based 3D printer. Different dispersant concentrations and solid loadings were investigated, and a ZrO_2 slurry with a solid loading of 42 vol% was found to be suitable for DLP. After sintering at 1500 °C for 3 h, the properties obtained were found to be similar to those of ZrO_2 prepared through dry pressing. Sun et al. [29] studied the optimization of slurry and debinding processes during DLP 3D printing of yttria-stabilized zirconia. Their study revealed that an 83 % solid loading of zirconia was beneficial for the DLP process. In the debinding process, a heating rate of 0.2 °C/min was found to produce defect-free parts. Shi et al. [30] investigated the 3D inkjet printing of 3Y-TZP for dental applications. A ceramic ink with a solid loading of 55 % and a printing speed of 15 mm/s were found to be stable and efficient for 3D printing. However, the printed parts were rough because of the large filament diameter of 0.5 mm. Gnanasagaran et al. [31] evaluated the microstructural and mechanical properties of 3Y-TZP fabricated using fused deposition modelling (FDM) and compared the results with those obtained using the slip-casting method. The parts fabricated through FDM were

found to have a lower density and lower strength than those fabricated using the slip-casting method. Zhang et al. [32] 3D printed a dental implant with a lamellar surface topography from a zirconia ceramic using ink jetting. The 3D-printed implant exhibited good compressive strength owing to its dense core and supported osseointegration owing to the lamellar surface pores. Thus, AM of zirconia ceramics offers various advantages and is an attractive option, especially for dental applications, as it can enable the fabrication of dental prostheses with less material waste and customized geometries. In this study, we fabricated fully dense 3Y-TZP zirconia using DLP 3D printing. The shrinkage ratios, densities, X-ray diffraction (XRD) peaks, and surface integrity of the samples were determined after debinding and sintering. The mechanical properties of the sintered specimens were evaluated using four-point bending, tensile, and compression tests.

2. Material and methods

2.1. Slurry preparation

Zirconia powder (3 mol% yttria–partially stabilized tetragonal zirconia polycrystals (3Y-TZP)) with 99.9 % purity was used to prepare the slurry. The zirconia powder and liquid binder were stirred and mixed in a mixer at high speed to form a slurry. The liquid binder was composed of photoinitiator, monomer, oligomer, and additive components. The photoinitiator facilitates the radical reaction and polymerization of the UV binder. The difunctional monomer has a low viscosity, which enables the zirconia powder to be mixed at a high weight. The oligomer component has the microstructure of aliphatic urethane acrylate and facilitates a flexible and strong combination of liquid zirconia layers. The additive is a dispersing agent that facilitates the homogeneous distribution of zirconia powder in the liquid binder and ensures the appropriate viscosity and rheological properties. Table 1 summarizes the slurry compositions.

2.2. DLP 3D printing of zirconia

Zirconia samples were 3D printed using a DLP 3D printer (Zipro, AON, South Korea) shown in Fig. 1(a). A schematic of DLP 3d printing process is shown in Fig. 1(b). The specimen STL files were imported into the slicing software for orientation, scaling, support generation, slicing, and build file preparation. The zirconia slurry was poured into the slurry tank and spread on the build plate using a leveler. The UV light from the projector selectively photo-cured the slurry based on the slicing data. After each layer was built, the build table was lowered based on the selected layer thickness, and the process was repeated until the last layer. After completion of the build, the build plate was dipped in isopropyl alcohol for a few minutes to remove the uncured slurry adhering to the parts. The parts were detached from the build plate by removing the supports attached to the build plate using tweezers. The supports were removed, and the support marks were polished using grinding/polishing paper. The parts were then dried in ambient air.

2.3. Debinding and sintering

The as-built parts are in the green state; thus, they require debinding and sintering to remove the binders and become fully dense [33]. Debinding depends on factors such as the composition, component geometry, and solid loading. Thermogravimetric analysis (TGA) and differential thermogravimetry (DTG) of the green bodies were performed using a synchronous thermal analyzer (Lonory, China). Fig. 2 shows the TGA and DTG curves of the as-built green part. The decomposition starts at 261.6 °C and ends at 507.2 °C. Three decomposition peaks are observed at approximately 304.2, 396.9, and 465 °C. The final decomposition temperature of the cured slurry is approximately 486.9 °C. The TGA curve shows that approximately 85.42 % of the material is stable at 600 °C, which indicates the composition of zirconia powder. Based on the TGA/DTG data, a debinding cycle was designed as shown in Fig. 3. The debinding temperature scheme should be designed such that it allows the removal of gases generated by the decomposition of binding agents present in the slurry. Inappropriate debinding schemes can lead to cracks in the final sintered parts. Debinding and sintering were performed in a muffle furnace (Tigerspeed, Tiger, South Korea) using the program cycle listed in Table 2.

During debinding, the parts were initially heated to 200 °C at a high heating rate. From 200 °C to 320 °C, the parts were heated gradually at a rate of 0.025 °C/min and then held at 320 °C for 1 h. Because most of the decomposition occurs during this stage, it is important to perform the debinding at a slower rate to facilitate the removal of gases formed during decomposition. From 320 °C to 490 °C, the parts were heated at 0.25 °C/min and then held at 490 °C for 1 h. Because the final decomposition temperature is around 490 °C, the parts were heated at 10 °C/min from 490 °C to 1500 °C. Finally, the parts were sintered at 1500 °C for 2 h followed by allowing the furnace to cool.

Table 1
Slurry composition.

Material	weight (%)
Photoinitiator	0.1–2
Monomer	8–15
Oligomer	2–8
Additive	0.1–3
Zirconia	85

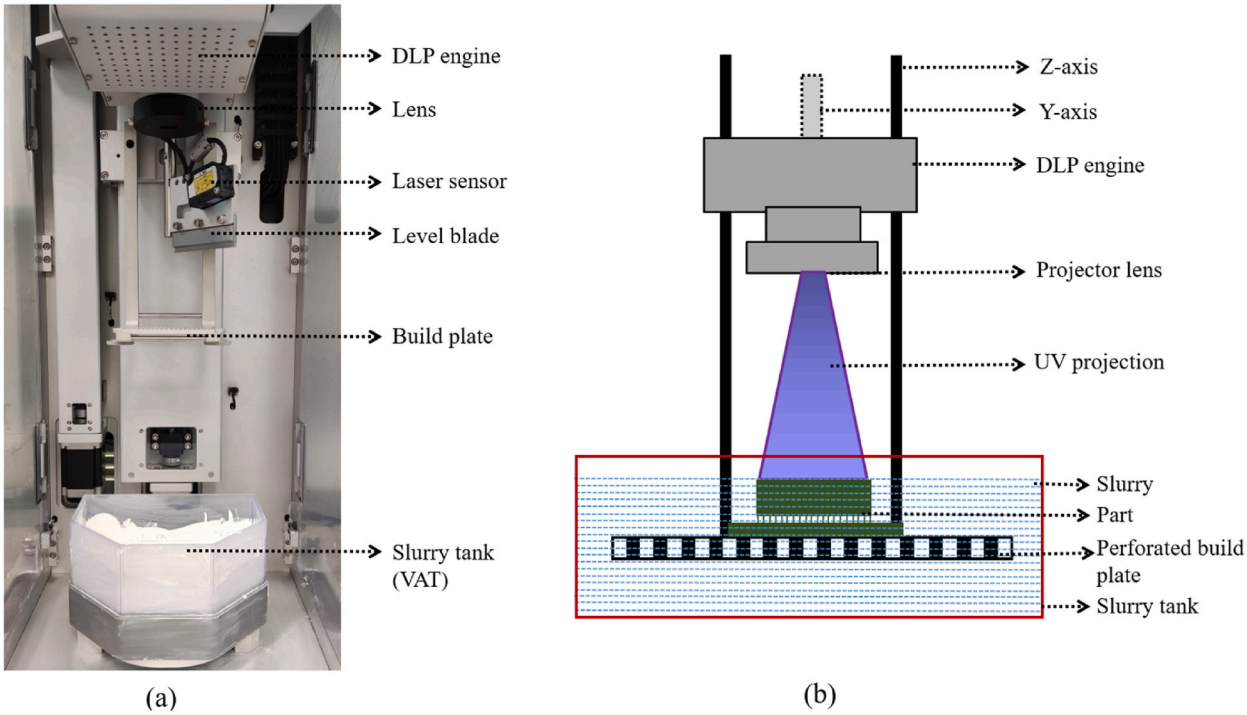

Fig. 1. (a) DLP 3D printing setup; (b) schematic diagram.

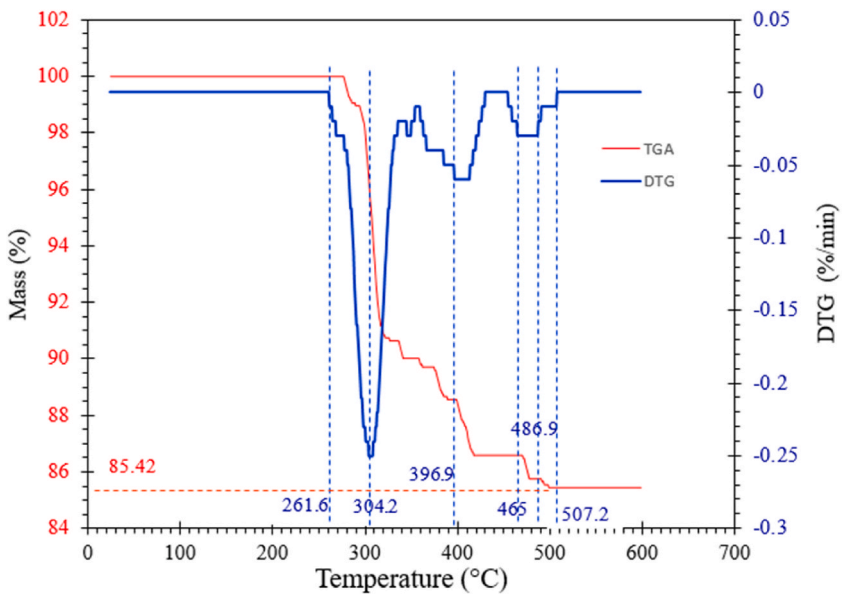

Fig. 2. TGA and DTG curves of the as-built part.

2.4. Characterization

The as-built parts tend to shrink after debinding and sintering. Five cuboid samples with dimensions of 5 × 6 × 15 mm were fabricated and subjected to the debinding and sintering schedule over 97 h and 25 min to evaluate the shrinkage and subsequent scaling ratios in the x, y, and z directions. Fig. 3 illustrates the fabrication process of the specimens. The model STL files were pre-possessed in the slicer software to generate build file as shown in Fig. 3(a). DLP 3d printing was carried out using the slicing data as shown in Fig. 3(b). The parts were cleaned using isopropyl alcohol to remove the uncured slurry as shown in Fig. 3(c). The parts were

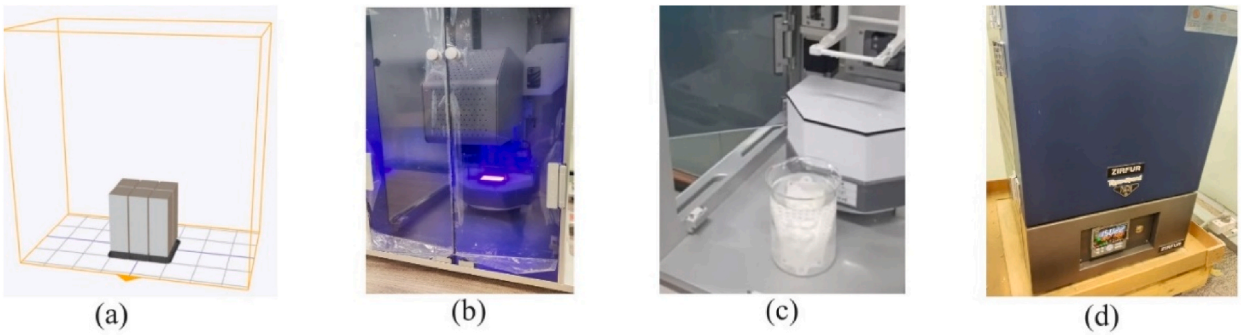

Fig. 3. Illustration of the fabrication of cuboid specimens: (a) part orientation and slicing, (b) 3D printing, (c) cleaning, (d) debinding and sintering.

Table 2
Debinding and sintering schedule.

Step	Start Temp (°C)	End Temp (°C)	Ramp Rate (°C/min)	Time (min)	Total Time
1	20	150	10	13	97 h 23 min
2	150	200	5	10	
3	200	320	0.025	4800	
4	320	320	–	60 (hold)	
5	320	490	0.25	680	
6	490	490	–	60 (hold)	
7	490	1500	10	100	
8	1500	1500	–	120 (hold)	
Furnace cooling					

then subjected to debinding and sintering as shown in Fig. 3(d). The density of the sintered parts was calculated using the Archimedes principle with a Sartorius secura224-1s precision weighing balance (Sartorius Lab Instruments, Germany). The surface integrity was evaluated using a Surtronics s100 instrument (Taylor Hobson, UK). XRD analysis of the as-built and sintered specimens was performed using a D2 Phaser X-ray diffractometer (Bruker, Germany). The Vickers hardness was measured using a Zwick microhardness tester with a load of 500 g for a dwell time of 20 s.

The sintered samples were ground and finely polished using Ecomet 30 (Buehler, Germany). The polished samples were heated in a

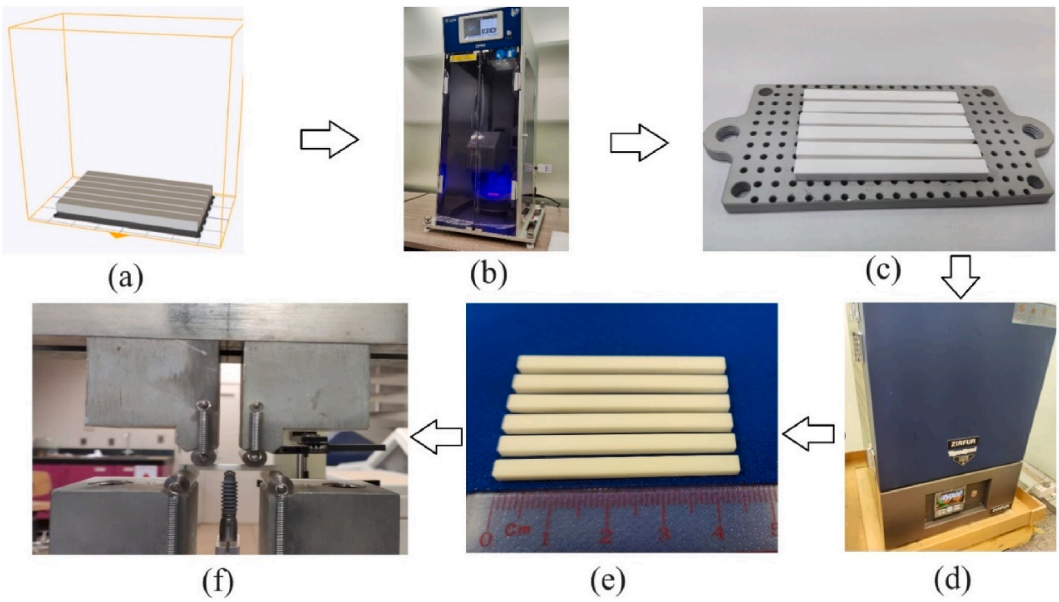

Fig. 4. (a) Support generation and slicing, (b) 3D printing, (c) support removal and cleaning, (d) debinding and sintering, (e) sintered samples, and (f) four-point bending test.

furnace at 10 °C/min from room temperature to 1350 °C. Thermal etching was performed by holding the samples at 1350 °C for 10 min to reveal the microstructure and grains. SEM was performed using a Tescan Vega instrument (Czech Republic).

2.5. Flexural strength

The flexural strengths of the specimens were determined via four-point bending tests with a universal testing machine (Hounsfield h100ks, Hounsfield Test Equipment, UK). Tests were performed on six specimens according to the ASTM C1161 standard, with sample dimensions of 45 × 4 × 3 mm, an inner span of 20 mm, outer span of 40 mm, and strain rate of 0.5 mm/min. Fig. 4 shows the sample fabrication and flexural test setup. The sample STL files were preprocessed in the slicer for support generation and build file preparation (Fig. 4(a)). The samples were 3d printed using the sliced data (Fig. 4(b)). After the completion of the build, the support structures were removed, and samples were cleaned using isopropyl alcohol and dried in the ambient air (Fig. 4(c)). The samples were then placed in the furnace for debinding and sintering (Fig. 4(d)) to become fully dense and attain their full strength (Fig. 4(e)). The samples were subjected to four-point bending setup to determine the flexural strength as shown in Fig. 4(f). The load was applied until failure of the sample, and the maximum load was utilized to calculate the flexural strength, σf. Because the inner span is exactly half the total span, the flexural strength is expressed using Equation (1).

$$\sigma_f = \frac{3Fl}{4bd^2}, \tag{1}$$

where F is the maximum load, l is the support span, and b and d are the width and thickness of the sample, respectively.

2.6. Tensile tests

Tensile tests were performed using a universal testing machine (Zwick/Roell Z100, Germany) as shown in Fig. 5(a). The specimen dimensions based on modified ASTM C 1273–05 were as follows: a width of 3 mm, thickness of 2.5 mm, and gauge length of 20 mm. Tests were performed on five specimens; the load was applied at 1 mm/min until failure of the specimens. Fig. 5(b) shows the test specimen subjected to tensile loading. Fig. 5(c) shows the sintered test specimens.

2.7. Compression tests

Compression tests were performed using a universal testing machine (Zwick/Roell Z100, Germany). The specimen had a diameter of 6.35 mm and length of 12.7 mm based on the ASTM C 773 test method. The tests were performed on four specimens at a rate of 0.25 mm/min until failure. Fig. 6(a) shows the as-built and sintered test specimens. Fig. 6(b) shows the sintered specimen subjected to compressive loading.

3. Results and discussion

3.1. Physical properties

To achieve the desired dimensions of the part after sintering, the parts were scaled up during design and fabrication. To determine

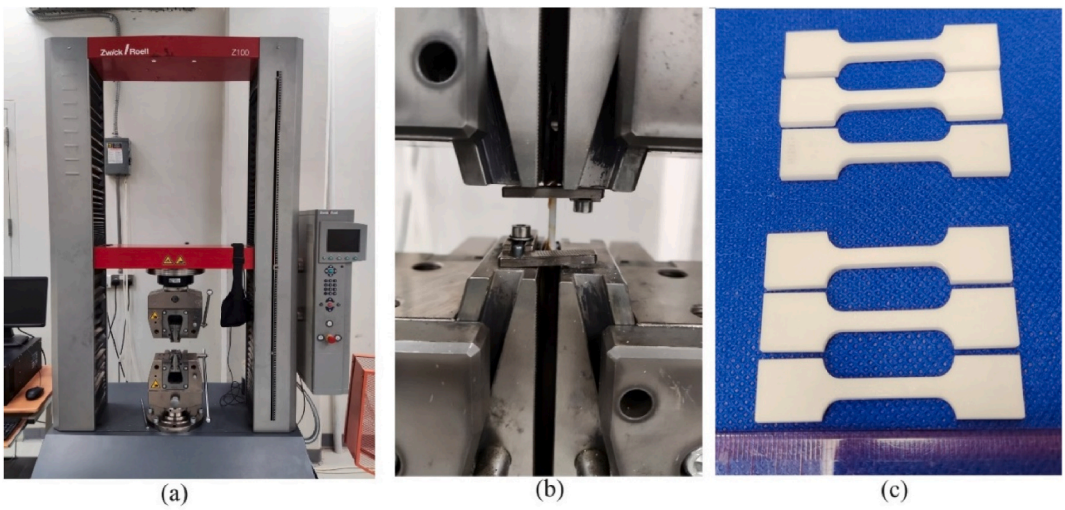

Fig. 5. (a) Universal testing machine, (b) enlarged view of the setup, (c) sintered tensile test specimens.

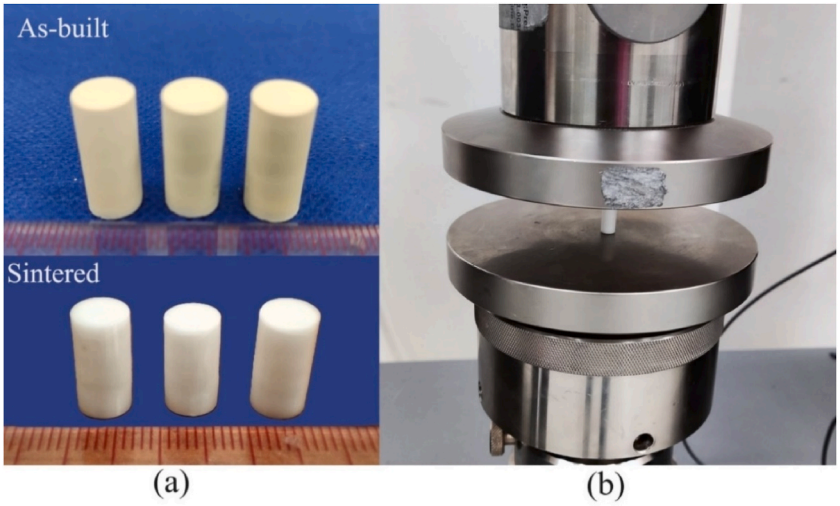

Fig. 6. (a) Compression test specimens in the as-built form and after sintering, (b) test setup.

the scaling factor, sample dimensions were measured before and after sintering. Fig. 7 shows an as-built sample in the green state and the corresponding sintered sample. It can be seen that the sample shrank in all directions. The dimensions of the as-built samples were measured in the x, y, and z directions using Vernier calipers and were compared with those of the sintered samples. The average shrinkages in the x, y, and z directions were 22.11 %, 22.51 %, and 25.31 %, respectively. The scaling ratio in each direction was calculated as Lg/Ls, where Lg is the dimension in the green state and Ls is the dimension after sintering. The average scaling ratios in the x, y, and z directions were 1.2839, 1.2906, and 1.3390, respectively. Table 3 lists the average dimensions of the samples before and after sintering, along with the scaling ratios. Fig. 8(a) and (b) shows microscopic images of the side surfaces of the as-built and sintered samples. It can be seen that the 50 μm layer thickness in the as-built sample shrank to approximately 37 μm in the sintered sample, which indicates the shrinkage in the z-direction.

The density of the sintered part, ρ_s, was calculated based on Equation (2), where w_{air} is the weight of the sample in air, w_{water} is the

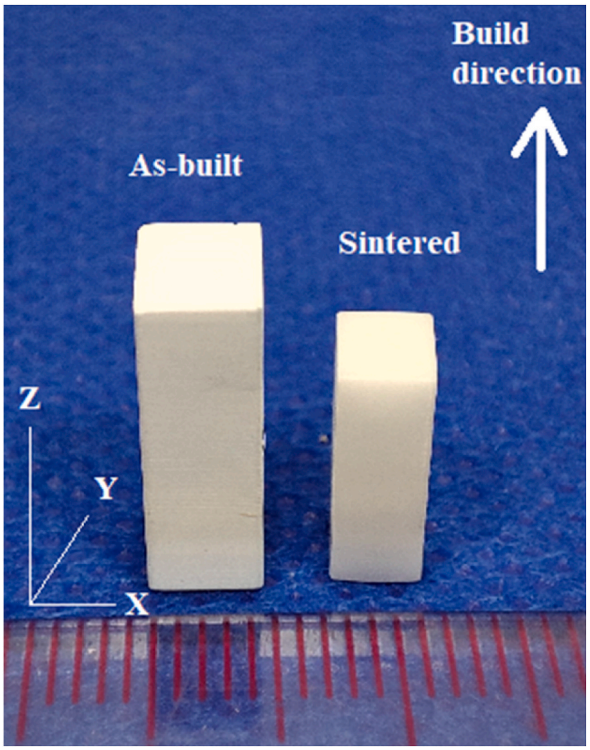

Fig. 7. Cuboid specimen in the as-built condition and after sintering.

weight of the sample in water, and ρ_{Water} is the density of water. Fig. 9(a) shows the sample measurements in air and Fig. 9(b) shows the sample measurements in water. Distilled water with a density of 0.9982 g/cc was used for these measurements. Five sample measurements were performed, and the average density was 6.031 ± 0.03 g/cc. The density of the 3D-printed zirconia (6.031 ± 0.03 g/cc) was comparable to that of commercially available bulk zirconia (5.85–6.10 g/cc). The Vickers microhardness tests results showed an average hardness of the sintered sample to be approximately 1059 ± 27 HV. This is much higher than the hardness of many other dental materials [34] and is similar to that of pre-sintered zirconia blocks [35,36].

$$\rho_s = \left(\frac{w_{air}}{w_{air} - w_{water}}\right) * \rho_{Water}. \tag{2}$$

The roughness of the top and side surfaces of the sintered samples was tested. Fig. 10 shows the profile of the side surface. The average Ra values of the top and side surfaces were 1.05 μm and 3.49 μm, respectively. The top surface was found to have a better surface quality than the side surface. The side surface was rough because of the layering effect. However, the surface finish can be improved by polishing the as-built parts. Because the as-built parts are in the green state, they can be easily polished using grinding and polishing tools before debinding and sintering to achieve smooth surfaces.

3.2. XRD

The XRD pattern of the sintered zirconia shows typical changes from the as-built condition, as reported in the literature. A comparison of the patterns of the as-built and sintered specimens shows a predominant tetragonal phase in the sintered specimen compared with the monoclinic phase in the as-built specimen, as shown in Fig. 11. The as-built specimen contained predominant monoclinic phases and some tetragonal phases, whereas the sintered specimen exhibited a tetragonal phase with negligible monoclinic phases. This is because the monoclinic phase of ZrO_2 is transformed into the tetragonal phase during sintering at 1500 °C, and it is stable owing to the yttria content.

3.3. SEM analysis

SEM analysis shows the surface characteristics and microstructure of the sintered specimen. It can be seen in Fig. 12(a) that the samples are uniformly sintered and fully dense across the layer. The samples are free from defects such as micro cracks and voids which indicates the efficiency of the debinding and sintering process. However, micro pores are observed in the sintered samples which are usually found in 3d printed zirconia. Micro pores are mainly due to the air bubbles entrapped in the slurry during 3d printing due its high viscosity as reported in the previous studies [37,38]. Fig. 12(b) shows the microstructure and grains of the sintered specimen. It can be seen that the grains are in tight arrangement with the average grain size of 0.35 ± 0.1 μm.

3.4. Flexural strength

Four-point flexural tests were performed to evaluate the flexural strength of the 3D-printed zirconia. In the four-point flexural test, the specimen was placed between the loading spans, and the stress was uniformly distributed between the spans. Table 4 lists the force, displacement, and strength data of the test specimens. Fig. 13 shows the flexural strengths of the test specimens. The average flexural strength of the sintered specimens was 451.876 MPa, which is consistent with previously published results [39–41]. The flexural values in the present study are slightly lower than those in the literature; however, it should be noted that these are four-point flexural results, whereas the values in the literature were mostly obtained using three-point flexural tests. The flexural strength values in four-point flexural tests will be significantly lower than those in three-point flexural tests. However, four-point flexure is preferred and recommended for characterization because it exposes a larger portion of the material being tested [42]. The average chewing force has been reported to be in the range of 40–440 N. Therefore, the flexural strength required for dental restorations such as veneers, single crowns, and inlays is 200 MPa [43]. These results show that the 3D-printed zirconia is suitable for dental applications.

3.5. Tensile strength

The tensile stress–strain curves for five sintered zirconia samples subjected to tensile loading are shown in Fig. 14. It should be noted that the strain in the curves does not represent the true strain, and slippage of the gripping surfaces may occur. However, the curves are similar to typical brittle fracture curves. At the initial stage of the curves, the slope increases gradually, which indicates micro-fractures and deformation of the internal defects. During the second stage of the curves, the slope increases linearly, which can be attributed to the stable evolution of microcracks. In one of the samples, after the second stage, a linear to nonlinear transition in the

Table 3
Average dimensions of the green and sintered samples along with the scaling ratio.

Direction	Lg (mm)	Ls (mm)	Scaling ratio
x	5.02	3.91	1.2839
y	6.04	4.68	1.2906
z	15.05	11.24	1.3390

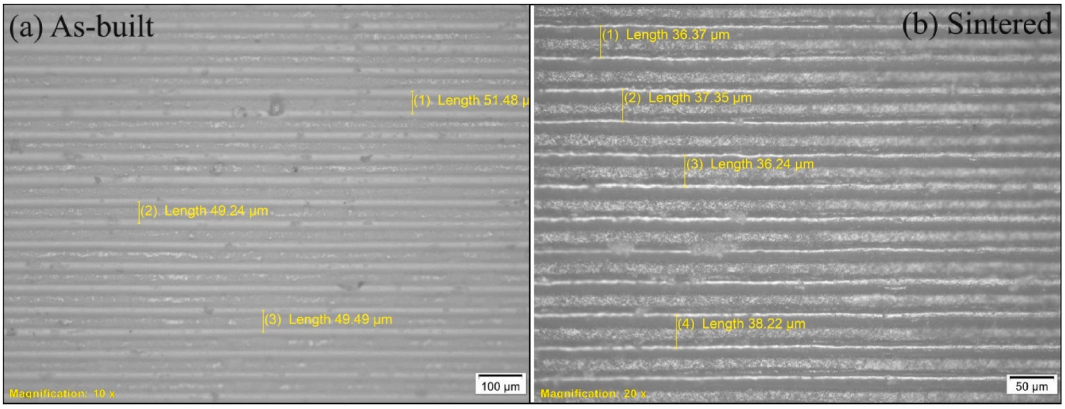

Fig. 8. Microscopic images of the side surface of a specimen: (a) as-built, (b) after sintering.

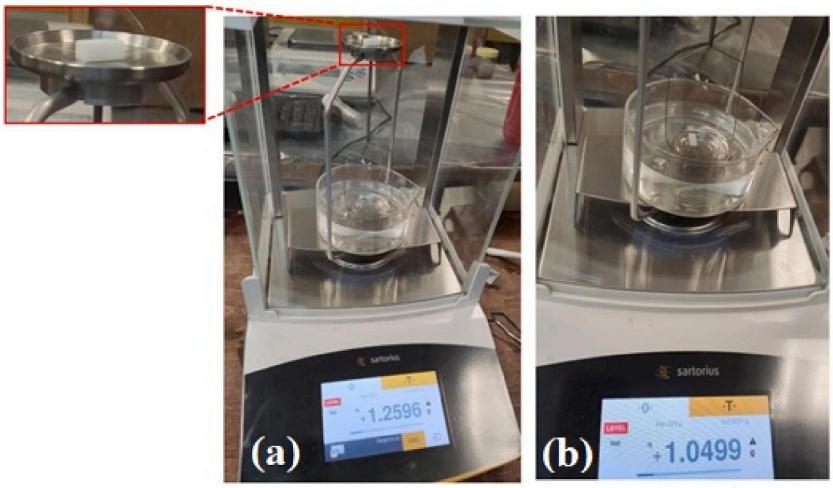

Fig. 9. (a) Weight in air, (b) weight in water.

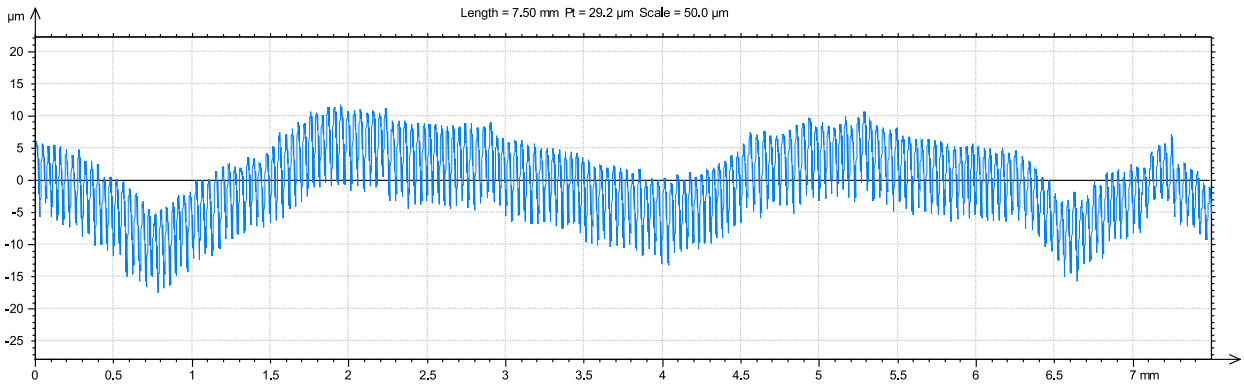

Fig. 10. Surface profile of the side surface of the sintered specimen.

curve was observed, which indicates a rapid propagation of the microcracks. After reaching the peak stress, the specimen fractured suddenly along with a crisp sound, which is typical of a brittle fracture. The tensile stress level at which the specimen fractured was recorded as the ultimate tensile strength of the specimen. The average ultimate tensile strength (UTS) of the 3D-printed sintered zirconia was 143 MPa.

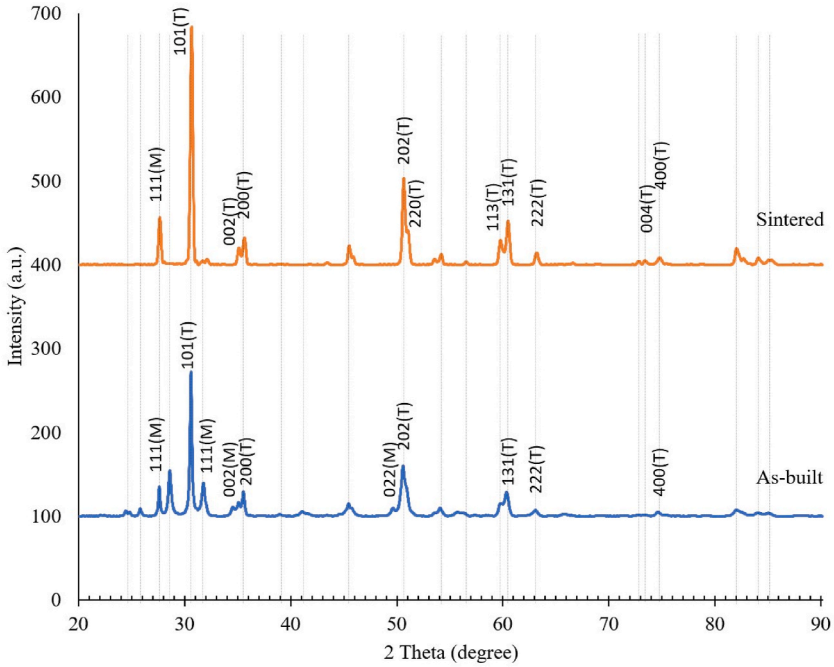

Fig. 11. XRD patterns of as-built and sintered specimens.

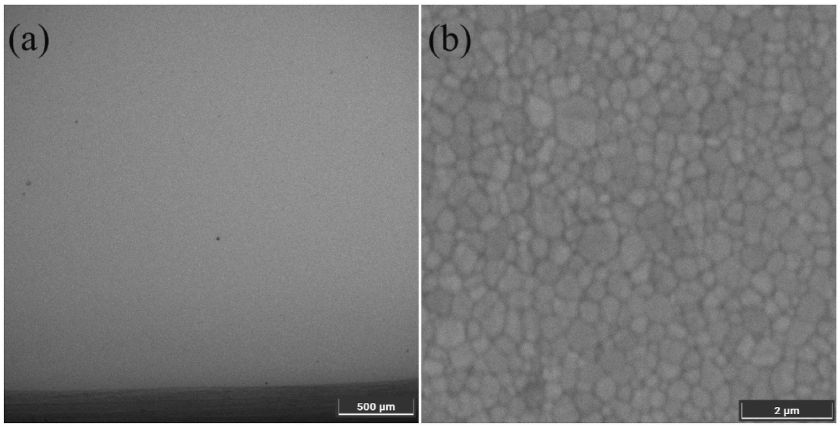

Fig. 12. SEM images of the sintered specimen: (a) surface characteristics, (b) microstructure.

Table 4
Force displacement and strength data for flexural samples.

	Extension (mm)	Force (N)	σ (MPa)
1	0.354	614.33	500.184
2	0.33	556.50	453.097
3	0.44	546.00	444.548
4	0.41	562.50	457.982
5	0.48	508.67	414.152
6	0.422	542.00	441.291
		Average	451.876

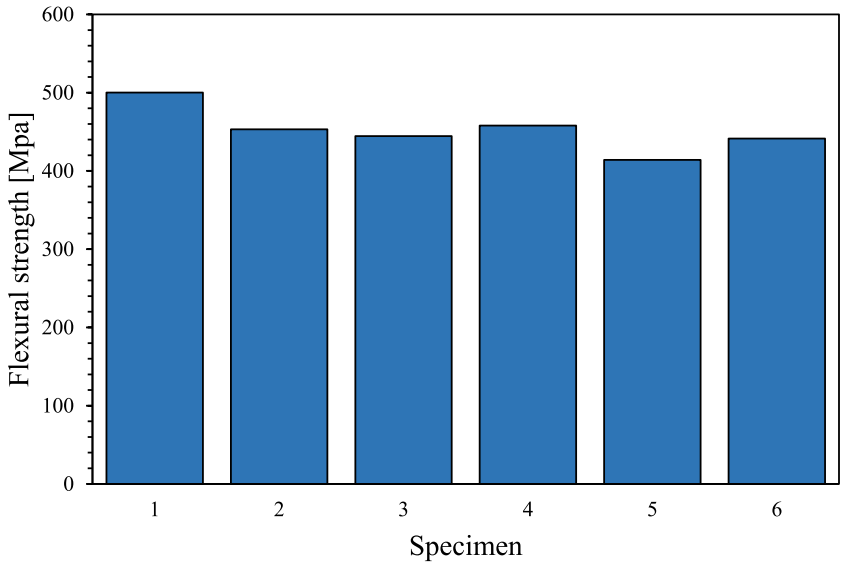

Fig. 13. Flexural strengths of test specimens.

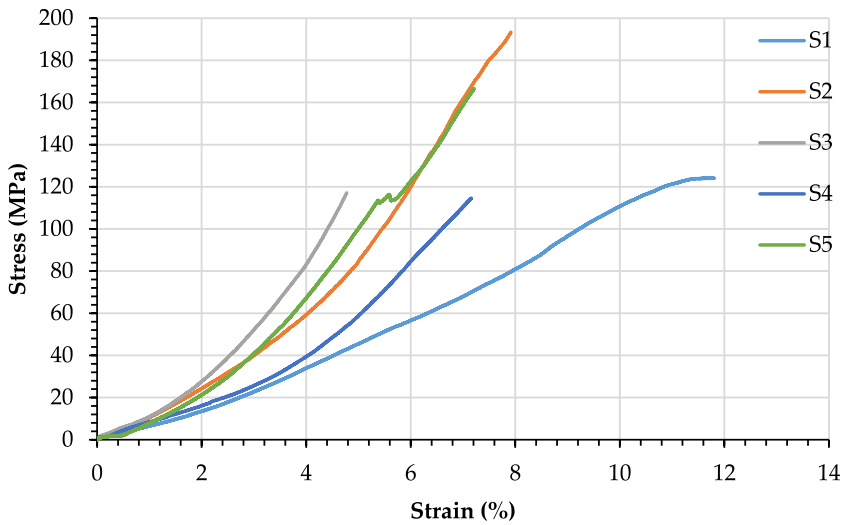

Fig. 14. Stress–strain curves of tensile specimens.

3.6. Compressive strength

Fig. 15 shows the stress–strain curves for sintered zirconia samples subjected to compressive loading. The compressive stress–strain curves exhibit three regions. In the first region, the slope of the stress–strain curve increases gradually, which can be attributed to micro-fractures and deformation. The second stage is the linear elastic region, in which the stress increases linearly and reaches a peak. This is followed by the fracture point, beyond which the specimen fails abruptly with a crisp sound, which is characteristic of a brittle fracture. The average compressive strength was 298.4 MPa, whereas the average modulus was 13.05 GPa. The compressive strength of the 3D-printed zirconia in this study was lower than that of bulk zirconia, which was reported to be approximately 2000 MPa [44]. This is because of the cracks and internal porosity of the specimen. The presence of defects in the compressive test specimens could be attributed to the expansion of gases released during debinding because of the decomposition of the binding agent, which induced cracks in the specimen. This is more significant in the case of thicker specimens, such as the compressive test specimens. Further research is required to optimize the debinding and sintering schedule to produce larger parts that are free from defects.

Fig. 16 shows 3D-printed dental prosthesis made of zirconia ceramics. It can be seen that the complex surfaces of veneers and crowns were fabricated successfully without any defects. Because the veneers and crowns are small and have thin surfaces, the strength achieved after debinding and sintering will be much higher than the test results for the standard specimens. A detailed analysis of the fabricated veneers and crowns on a chewing simulator should be performed in a future study to fully assess the strength and properties

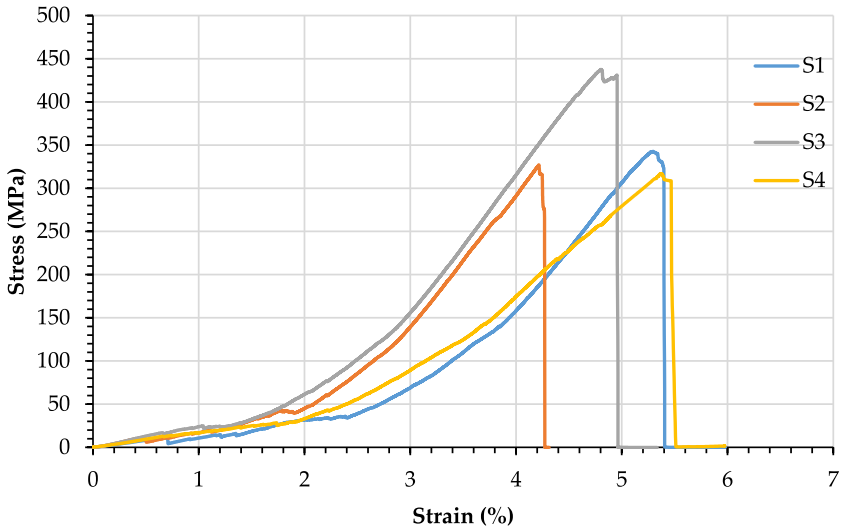

Fig. 15. Stress–strain curves of compressive test specimens.

of the prosthesis.

4. Conclusions

Zirconia ceramic parts were fabricated using a DLP 3D printing process and sintered at 1500 °C to obtain fully dense parts for dental applications. The as-built parts were subjected to TGA/DTG tests to determine their decomposition temperatures and design the debinding process. The shrinkage, density, and surface roughness of the sintered parts were investigated. The mechanical properties of the specimens were determined using microhardness, flexural strength, tensile strength, and compressive strength tests. The main conclusions drawn from this study are as follows.

- The TGA/DTG curves indicate the final decomposition temperature of the slurry was 486.9 °C. Approximately 85.42 % of the material was stable at 600 °C, which indicates the composition of zirconia.
- Debinding and sintering of the specimens were performed using a one-step process in a muffle furnace at low heating rates for approximately 97 h 25 min. The sintered parts were free from defects such as delamination and cracks.

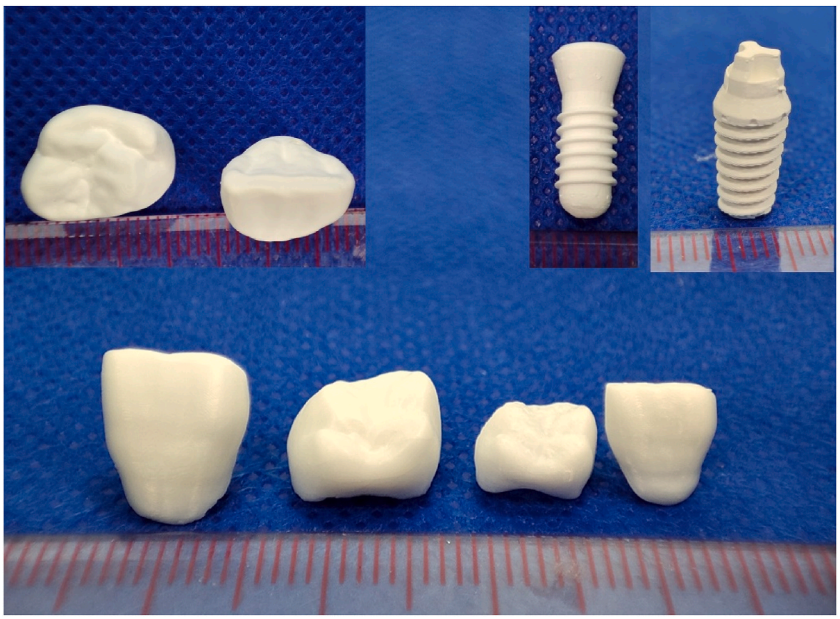

Fig. 16. 3D-printed dental prostheses.

- Sintering of the specimens resulted in shrinkage. The average shrinkages of the specimens in x, y, and z direction were 22.11 %, 22.51 %, and 25.31 %, respectively. The scaling factors were thus 1.2839, 1.2906, and 1.3390 in the x, y, and z directions, respectively.
- The average density of the sintered parts, determined using Archimedes' principle, was 6.031 g/cc. Vickers microhardness tests revealed that the average microhardness of the sintered samples was 1046 HV.
- The XRD patterns of the sintered zirconia samples showed a prevalent tetragonal phase in the sintered samples and the transformation of the monoclinic phase in the as-built sample to the tetragonal phase after sintering.
- The flexural strength of the sintered zirconia samples, determined using four-point bending tests, was 451.876 MPa.
- The average UTS of the fabricated specimens was 143 MPa.
- The average compressive strength of the specimens was 298.4 MPa, and the modulus was 13.05 GPa.

Funding

The authors extend their appreciation to the Deputyship for Research & Innovation, "Ministry of Education" in Saudi Arabia for funding this research work through the project number (IFKSUDR_D105).

Data availability statement

All the data supporting the findings of this study is available within the article. Further information is available from the corresponding author upon reasonable request.

CRediT authorship contribution statement

Muneer Khan Mohammed: Writing – review & editing, Writing – original draft, Validation, Resources, Methodology, Investigation, Funding acquisition, Formal analysis, Conceptualization. **Abdulrahman Alahmari:** Writing – review & editing, Supervision, Methodology, Funding acquisition, Formal analysis, Conceptualization. **Hisham Alkhalefah:** Writing – original draft, Validation, Supervision, Resources, Investigation. **Mustufa Haider Abidi:** Writing – review & editing, Writing – original draft, Validation, Methodology, Investigation, Formal analysis.

Declaration of competing interest

The authors declare that they have no known competing financial interests or personal relationships that could have appeared to influence the work reported in this paper.

Acknowledgments

The authors extend their appreciation to the Deputyship for Research & Innovation, "Ministry of Education" in Saudi Arabia for funding this research work through the project no. (IFKSUDR_D105).

References

[1] M.H. Ghaemi, S. Reichert, A. Krupa, M. Sawczak, A. Zykova, K. Lobach, S. Sayenko, Y. Svitlychnyi, Zirconia ceramics with additions of alumina for advanced tribological and biomedical applications, Ceram. Int. 43 (2017) 9746–9752, https://doi.org/10.1016/j.ceramint.2017.04.150.
[2] R.B. Osman, A.J. van der Veen, D. Huiberts, D. Wismeijer, N. Alharbi, 3D-Printing zirconia implants; a dream or a reality? An in-vitro study evaluating the dimensional accuracy, surface topography and mechanical properties of printed zirconia implant and discs, J. Mech. Behav. Biomed. Mater. 75 (2017) 521–528, https://doi.org/10.1016/j.jmbbm.2017.08.018.
[3] L. Hanafi, M. Altinawi, J.C. Comisi, Evaluation and comparison two types of prefabricated zirconia crowns in mixed and primary dentition: a randomized clinical trial, Heliyon 7 (2021) e06240, https://doi.org/10.1016/j.heliyon.2021.e06240.
[4] Y. Zhang, B.R. Lawn, Novel zirconia materials in dentistry, J. Dent. Res. 97 (2018) 140–147, https://doi.org/10.1177/0022034517737483.
[5] R.H.J. Hannink, P.M. Kelly, B.C. Muddle, Transformation toughening in zirconia-containing ceramics, J. Am. Ceram. Soc. 83 (2000) 461–487, https://doi.org/10.1111/j.1151-2916.2000.tb01221.x.
[6] A. Kui, M. Manziuc, A. Petruțiu, S. Buduru, A. Labuneț, M. Negucioiu, A. Chisnoiu, Translucent zirconia in fixed prosthodontics-an integrative overview, Biomedicines 11 (2023) 3116, https://doi.org/10.3390/biomedicines11123116.
[7] I. Denry, J.R. Kelly, State of the art of zirconia for dental applications, Dent. Mater. 24 (2008) 299–307, https://doi.org/10.1016/j.dental.2007.05.007.
[8] P.F. Manicone, P. Rossi Iommetti, L. Raffaelli, An overview of zirconia ceramics: basic properties and clinical applications, J. Dent. 35 (2007) 819–826, https://doi.org/10.1016/j.jdent.2007.07.008.
[9] H. Warashina, S. Sakano, S. Kitamura, K.-I. Yamauchi, J. Yamaguchi, N. Ishiguro, Y. Hasegawa, Biological reaction to alumina, zirconia, titanium and polyethylene particles implanted onto murine calvaria, Biomaterials 24 (2003) 3655–3661, https://doi.org/10.1016/S0142-9612(03)00120-0.
[10] M. Degidi, L. Artese, A. Scarano, V. Perrotti, P. Gehrke, A. Piattelli, Inflammatory infiltrate, microvessel density, nitric oxide synthase expression, vascular endothelial growth factor expression, and proliferative activity in peri-implant soft tissues around titanium and zirconium oxide healing caps, J. Periodontol. 77 (2006) 73–80, https://doi.org/10.1902/jop.2006.77.1.73.
[11] F. Carinci, F. Pezzetti, S. Volinia, F. Francioso, D. Arcelli, E. Farina, A. Piattelli, Zirconium oxide: analysis of MG63 osteoblast-like cell response by means of a microarray technology, Biomaterials 25 (2004) 215–228, https://doi.org/10.1016/S0142-9612(03)00486-1.
[12] A.-R. Alao, R. Stoll, X.-F. Song, T. Miyazaki, Y. Hotta, Y. Shibata, L. Yin, Surface quality of yttria-stabilized tetragonal zirconia polycrystal in CAD/CAM milling, sintering, polishing and sandblasting processes, J. Mech. Behav. Biomed. Mater. 65 (2017) 102–116, https://doi.org/10.1016/j.jmbbm.2016.08.021.
[13] M. Amaral, R.F. Villefort, R.M. Melo, G.K.R. Pereira, Y. Zhang, L.F. Valandro, M.A. Bottino, Fatigue limit of monolithic Y-tzp three-unit-fixed dental prostheses: effect of grinding at the gingival zone of the connector, J. Mech. Behav. Biomed. Mater. 72 (2017) 159–162, https://doi.org/10.1016/j.jmbbm.2017.03.002.

[14] M. Inokoshi, F. Zhang, J. De Munck, S. Minakuchi, I. Naert, J. Vleugels, B. Van Meerbeek, K. Vanmeensel, Influence of sintering conditions on low-temperature degradation of dental zirconia, Dent. Mater. 30 (2014) 669–678, https://doi.org/10.1016/j.dental.2014.03.005.
[15] Z.M. Jassim, M.A. Majeed, Comparative evaluation of the fracture strength of monolithic crowns fabricated from different all-ceramic CAD/CAM materials (an in vitro study), Biomed. Pharmacol. J. 11 (2018) 1689–1697.
[16] L.-C. Dârlău, Obtaining metal parts by additive manufacturing, as an alternative to traditional manufacturing methods – a review, Bull. Polytech. Inst. Iași Mach. Constr. Sect. 69 (2023) 61–80, https://doi.org/10.2478/bipcm-2023-0005.
[17] U. Lakshminarayan, S. Ogrydiziak, H.L. Marcus, Selective Laser Sintering of Ceramic Materials, 1990.
[18] J. Wilkes, Y. Hagedorn, W. Meiners, K. Wissenbach, Additive manufacturing of ZrO2-Al2O3 ceramic components by selective laser melting, Rapid Prototyp. J. 19 (2013) 51–57, https://doi.org/10.1108/13552541311292736.
[19] J. Ebert, E. Özkol, A. Zeichner, K. Uibel, Ö. Weiss, U. Koops, R. Telle, H. Fischer, Direct inkjet printing of dental prostheses made of zirconia, J. Dent. Res. 88 (2009) 673–676, https://doi.org/10.1177/0022034509339988.
[20] J. Moon, J.E. Grau, V. Knezevic, M.J. Cima, E.M. Sachs, Ink-jet printing of binders for ceramic components, J. Am. Ceram. Soc. 85 (2002) 755–762, https://doi.org/10.1111/j.1151-2916.2002.tb00168.x.
[21] S. Lamnini, H. Elsayed, Y. Lakhdar, F. Baino, F. Smeacetto, E. Bernardo, Robocasting of advanced ceramics: ink optimization and protocol to predict the printing parameters - a review, Heliyon 8 (2022) e10651, https://doi.org/10.1016/j.heliyon.2022.e10651.
[22] H. Wu, D. Li, Y. Tang, B. Sun, D. Xu, Rapid fabrication of alumina-based ceramic cores for gas turbine blades by stereolithography and gelcasting, J. Mater. Process. Technol. 209 (2009) 5886–5891, https://doi.org/10.1016/j.jmatprotec.2009.07.002.
[23] R. He, W. Liu, Z. Wu, D. An, M. Huang, H. Wu, Q. Jiang, X. Ji, S. Wu, Z. Xie, Fabrication of complex-shaped zirconia ceramic parts via a DLP- stereolithography-based 3D printing method, Ceram. Int. 44 (2018) 3412–3416, https://doi.org/10.1016/j.ceramint.2017.11.135.
[24] E. Özkol, A.M. Wätjen, R. Bermejo, M. Deluca, J. Ebert, R. Danzer, R. Telle, Mechanical characterisation of miniaturised direct inkjet printed 3Y-tzp specimens for microelectronic applications, J. Eur. Ceram. Soc. 30 (2010) 3145–3152, https://doi.org/10.1016/j.jeurceramsoc.2010.07.016.
[25] A. Licciulli, C. Esposito Corcione, A. Greco, V. Amicarelli, A. Maffezzoli, Laser stereolithography of ZrO2 toughened Al2O3, J. Eur. Ceram. Soc. 25 (2005) 1581–1589, https://doi.org/10.1016/j.jeurceramsoc.2003.12.003.
[26] R. Galante, C.G. Figueiredo-Pina, A.P. Serro, Additive manufacturing of ceramics for dental applications: a review, Dent. Mater. 35 (2019) 825–846, https://doi.org/10.1016/j.dental.2019.02.026.
[27] A. Scarano, M. Piattelli, S. Caputi, G.A. Favero, A. Piattelli, Bacterial adhesion on commercially pure titanium and zirconium oxide disks: an in vivo human study, J. Periodontol. 75 (2004) 292–296, https://doi.org/10.1902/jop.2004.75.2.292.
[28] F. Chen, H. Zhu, J.-M. Wu, S. Chen, L.-J. Cheng, Y.-S. Shi, Y.-C. Mo, C.-H. Li, J. Xiao, Preparation and biological evaluation of ZrO2 all-ceramic teeth by DLP technology, Ceram. Int. 46 (2020) 11268–11274, https://doi.org/10.1016/j.ceramint.2020.01.152.
[29] J. Sun, J. Binner, J. Bai, 3D printing of zirconia via digital light processing: optimization of slurry and debinding process, J. Eur. Ceram. Soc. 40 (2020) 5837–5844, https://doi.org/10.1016/j.jeurceramsoc.2020.05.079.
[30] Y. Shi, W. Wang, 3D inkjet printing of the zirconia ceramic implanted teeth, Mater. Lett. 261 (2020) 127131, https://doi.org/10.1016/j.matlet.2019.127131.
[31] C.L. Gnanasagaran, K. Ramachandran, N.H. Jamadon, V.H. Kumar, A. Muchtar, A. Pazhani, B. Ayaz, Microstructural and mechanical behaviours of Y-tzp prepared via slip-casting and fused deposition modelling (FDM), Heliyon 9 (2023) e21705, https://doi.org/10.1016/j.heliyon.2023.e21705.
[32] F. Zhang, B.C. Spies, E. Willems, M. Inokoshi, C. Wesemann, S.M. Cokic, B. Hache, R.J. Kohal, B. Altmann, J. Vleugels, et al., 3D printed zirconia dental implants with integrated directional surface pores combine mechanical strength with favorable osteoblast response, Acta Biomater. 150 (2022) 427–441, https://doi.org/10.1016/j.actbio.2022.07.030.
[33] X. Li, H. Zhong, J. Zhang, Y. Duan, H. Bai, J. Li, D. Jiang, Dispersion and properties of zirconia suspensions for stereolithography, Int. J. Appl. Ceram. Technol. 17 (2020) 239–247, https://doi.org/10.1111/ijac.13321.
[34] C. Nair, P. Dathan, S. Sb, A. Soman, Hardness of dental materials is an essential property that determines the life of restorations - an overview, Acta Sci. Dent. Scienecs (2022) 129–134, https://doi.org/10.31080/ASDS.2022.06.1523.
[35] R.X. de Freitas, C. dos Santos, B.X. de Freitas, B.G. Simba, ZrO2 pre-sintered blocks (3%mol-Y2O3) with color gradient for dental prostheses, Mater. Sci. Forum 930 (2018) 57–62, 10.4028/www.scientific.net/MSF.930.57.
[36] N.F. Amat, A. Muchtar, H.Z. Yew, M.S. Amril, R.L. Muhamud, Machinability of a newly developed pre-sintered zirconia block for dental crown applications, Mater. Lett. 261 (2020) 126996, https://doi.org/10.1016/j.matlet.2019.126996.
[37] W. Harrer, M. Schwentenwein, T. Lube, R. Danzer, Fractography of zirconia-specimens made using additive manufacturing (LCM) technology, J. Eur. Ceram. Soc. 37 (2017) 4331–4338, https://doi.org/10.1016/j.jeurceramsoc.2017.03.018.
[38] I. Buj-Corral, D. Vidal, A. Tejo-Otero, J.A. Padilla, E. Xuriguera, F. Fenollosa-Artés, Characterization of 3D printed yttria-stabilized zirconia parts for use in prostheses, Nanomaterials 11 (2021) 2942, https://doi.org/10.3390/nano11112942.
[39] J.M. Suominen, E.J. Frankberg, P.K. Vallittu, E. Levänen, J. Vihinen, T. Vastamäki, R. Kari, L.V.J. Lassila, Three-dimensional printing of zirconia: characterization of early stage material properties, Biomater. Investig. Dent. 6 (2019) 23–31, https://doi.org/10.1080/26415275.2019.1640608.
[40] S.-Y. Lee, C.-P. Jiang, Development of a three-dimensional slurry printing system using dynamic mask projection for fabricating zirconia dental implants, Mater. Manuf. Process. 30 (2015) 1498–1504, https://doi.org/10.1080/10426914.2014.984208.
[41] Y. Zhao, P. Li, P. Dong, Y. Zeng, J. Chen, Investigation on 3D printing ZrO2 implant abutment and its fatigue performance simulation, Ceram. Int. 47 (2021) 1053–1062, https://doi.org/10.1016/j.ceramint.2020.08.221.
[42] Standard test method for flexural strength of advanced ceramics at ambient temperature, Available online: https://www.astm.org/c1161-18r23.html. (Accessed 1 March 2024).
[43] J.R. Kelly, Ceramics in restorative and prosthetic dentistry, Annu. Rev. Mater. Sci. 27 (1997) 443–468, https://doi.org/10.1146/annurev.matsci.27.1.443.
[44] C. Piconi, G. Maccauro, Zirconia as a ceramic biomaterial, Biomaterials 20 (1999) 1–25, https://doi.org/10.1016/S0142-9612(98)00010-6.